

Article

Multi-Centered Solid-Phase Quasi-Intramolecular Redox Reactions of [(Chlorido)Pentaamminecobalt(III)] Permanganate—An Easy Route to Prepare Phase Pure CoMn_2O_4 Spinel

Fernanda Paiva Franguelli ^{1,2}, Éva Kováts ³, Zsuzsanna Czégény ¹, Laura Bereczki ¹, Vladimir M. Petruševski ⁴ , Berta Barta Holló ⁵ , Kende Attila Béres ^{1,6} , Attila Farkas ⁷ , Imre Miklós Szilágyi ²  and László Kótai ^{1,8,*} 

- ¹ Research Centre for Natural Sciences, Hungarian Academy of Sciences, Magyar Tudósok krt. 2, H-1117 Budapest, Hungary; fepaiva@gmail.com (F.P.F.); czegeny.zsuzsanna@ttk.hu (Z.C.); nagyne.bereczki.laura@ttk.hu (L.B.); beres.kende.attila@ttk.hu (K.A.B.)
 - ² Department of Inorganic and Analytical Chemistry, Budapest University of Technology and Economics, Műegyetem rakpart 3, H-1111 Budapest, Hungary; imre.szilagyai@mail.bme.hu
 - ³ Wigner Research Centre for Physics (RCP), 761 Institute for Solid State Physics and Optics, Konkoly-Thege Miklós út 29-33, H-1121 Budapest, Hungary; kovats.eva@wigner.mta.hu
 - ⁴ Faculty of Natural Sciences and Mathematics, Ss. Cyril and Methodius University, 1000 Skopje, North Macedonia; vladimirpetrusevski@yahoo.com
 - ⁵ Department of Chemistry, Biochemistry and Environmental Protection, Faculty of Sciences, University of Novi Sad, Trg Dositeja Obradovića 3, 21000 Novi Sad, Serbia; hbarta@uns.ac.rs
 - ⁶ Institute of Chemistry, ELTE Eötvös Loránd University, Pázmány Péter s. 1/A, H-1117 Budapest, Hungary
 - ⁷ Department of Organic Chemistry, Budapest University of Technology and Economics, Budafoki út 8, H-1111 Budapest, Hungary; farkas.attila@mail.bme.hu
 - ⁸ Deuton-X Ltd., Selmeci u. 89, H-2030 Érd, Hungary
- * Correspondence: kotai.laszlo@ttk.hu



Citation: Franguelli, F.P.; Kováts, É.; Czégény, Z.; Bereczki, L.; Petruševski, V.M.; Barta Holló, B.; Béres, K.A.; Farkas, A.; Szilágyi, I.M.; Kótai, L. Multi-Centered Solid-Phase Quasi-Intramolecular Redox Reactions of [(Chlorido)Pentaamminecobalt(III)] Permanganate—An Easy Route to Prepare Phase Pure CoMn_2O_4 Spinel. *Inorganics* **2022**, *10*, 18. <https://doi.org/10.3390/inorganics10020018>

Academic Editor: Moris S. Eisen

Received: 16 January 2022

Accepted: 30 January 2022

Published: 4 February 2022

Publisher's Note: MDPI stays neutral with regard to jurisdictional claims in published maps and institutional affiliations.



Copyright: © 2022 by the authors. Licensee MDPI, Basel, Switzerland. This article is an open access article distributed under the terms and conditions of the Creative Commons Attribution (CC BY) license (<https://creativecommons.org/licenses/by/4.0/>).

Abstract: We synthesized and structurally characterized the previously unknown $[\text{Co}(\text{NH}_3)_5\text{Cl}](\text{MnO}_4)_2$ complex as the precursor of CoMn_2O_4 . The complex was also deuterated, and its FT-IR, far-IR, low-temperature Raman and UV-VIS spectra were measured as well. The structure of the complex was solved by single-crystal X-ray diffraction and the 3D-hydrogen bonds were evaluated. The N-H...O-Mn hydrogen bonds act as redox centers to initiate a solid-phase quasi-intramolecular redox reaction even at 120 °C involving the Co(III) centers. The product is an amorphous material, which transforms into $[\text{Co}(\text{NH}_3)_5\text{Cl}]\text{Cl}_2$, NH_4NO_3 , and a todorokite-like solid Co-Mn oxide on treatment with water. The insoluble residue may contain $\{\text{Mn}_4^{\text{III}}\text{Mn}^{\text{IV}}_2\text{O}_{12}\}_n^{4n-}$, $\{\text{Mn}_5^{\text{III}}\text{Mn}^{\text{IV}}\text{O}_{12}\}_n^{5n-}$ or $\{\text{Mn}_6^{\text{III}}\text{O}_{12}\}_n^{6n-}$ frameworks, which can embed $2 \times n$ (Co^{II} and/or Co^{III}) cations in their tunnels, respectively, and $4 \times n$ ammonia ligands are coordinated to the cobalt cations. The decomposition intermediates decompose on further heating via a series of redox reactions, forming a solid $\text{Co}^{\text{II}}\text{Mn}^{\text{III}}_2\text{O}_4$ spinel with an average size of 16.8 nm, and gaseous N_2 , N_2O and Cl_2 . The CoMn_2O_4 prepared in this reaction has photocatalytic activity in Congo red degradation with UV light. Its activity strongly depends on the synthesis conditions, e.g., Congo red was degraded 9 and 13 times faster in the presence of CoMn_2O_4 prepared at 550 °C (in air) or 420 °C (under N_2), respectively.

Keywords: permanganate; ammine; quasi-intramolecular redox reaction; cobalt manganite catalyst; spinel; todorokite; photochemical degradation; Congo red

1. Introduction

Nanosized mixed transition metal-manganese oxides can be prepared by the controlled thermal decomposition of transition metal permanganate complexes that have reducing inorganic [1–6] or organic ligands [7,8]. For example, Mansouri et al. prepared a cobalt manganese oxide spinel (CoMn_2O_4) with excellent activity in the Fischer–Tropsch

fuel synthesis, by the thermal decomposition of the $[\text{Co}(\text{NH}_3)_4\text{CO}_3]\text{MnO}_4$ complex [6,9]; however, $[\text{Co}(\text{NH}_3)_4\text{CO}_3]\text{MnO}_4$ contains Co and Mn in a 1:1 atomic ratio. Thus, the decomposition product is probably a mixed $\text{Co}(\text{Co}_{0.5}\text{Mn}_{1.5})\text{O}_4$ spinel or a mixture of CoMn_2O_4 and Co_3O_4 . To prepare a phase pure CoMn_2O_4 spinel, we attempted to prepare the $[\text{Co}(\text{NH}_3)_6]\text{Cl}(\text{MnO}_4)_2$ (**compound 1-Mn**) precursor (Co:Mn = 1:2), but despite the existing analogous perchlorate ($[\text{Co}(\text{NH}_3)_6]\text{Cl}(\text{ClO}_4)_2$) (**compound 1-Cl**) [10], our efforts were not successful. Alvisi [10] supposed that an unidentified chlorine-containing aminocobalt permanganate complex prepared by Klobb [11] was identical with **compound 1-Mn**, however, our repeated experiments showed that the mentioned compound was $[\text{Co}(\text{NH}_3)_6]\text{Cl}_2(\text{MnO}_4)$ (**compound 2-Mn**) (Co:Mn = 1:1) [11]. Moreover, we were able to produce an aminocobalt(III) permanganate complex precursor with the expected Co:Mn = 1:2 ratio with the isolation of the formerly unknown $[\text{Co}(\text{NH}_3)_5\text{Cl}](\text{MnO}_4)_2$ complex (**compound 3-Mn**). This precursor complex was structurally and spectroscopically characterized and heated, as a result of which it transformed into CoMn_2O_4 in an expected quasi-intramolecular redox reaction between the oxidizing (Co^{III} and permanganate) and reducing (ammonia and chloride) components. The labels for the synthesized compounds and composites used in the paper are given in Table 1.

Table 1. Labels of compounds.

Compound	Label
$[\text{Co}(\text{NH}_3)_6]\text{Cl}(\text{MnO}_4)_2$	1-Mn
$[\text{Co}(\text{NH}_3)_6]\text{Cl}(\text{ClO}_4)_2$	1-Cl
$[\text{Co}(\text{NH}_3)_6]\text{Cl}_2(\text{MnO}_4)$	2-Mn
$[\text{Co}(\text{NH}_3)_5\text{Cl}](\text{MnO}_4)_2$	3-Mn
$[\text{Co}(\text{NH}_3)_5\text{Cl}](\text{ClO}_4)_2$	3-Cl
$[\text{Co}(\text{NH}_3)_5\text{Cl}]\text{ReO}_4)_2 \cdot n\text{H}_2\text{O}$	3-Re
$[\text{Co}(\text{NH}_3)_5\text{Cl}]\text{Cl}_2$	4

2. Results and Discussion

2.1. Synthesis and Properties of Compound 3-Mn

[Chlorido(pentaammine)cobalt(III)] permanganate (**compound 3-Mn**) has not been prepared previously, although Krestov and Yatsimirskii [12] calculated its thermodynamical properties. The analogous perchlorate compound $(\text{Co}(\text{NH}_3)_5\text{Cl})(\text{ClO}_4)_2$ (**compound 3-Cl**) is known [13] and can easily be prepared by heating the [(aqua)(pentaammine)cobalt(III)] triperchlorate solution in 1 M HCl. Unfortunately, this reaction route cannot be used to prepare **compound 3-Mn** due to the spontaneous reaction between the permanganate ions and the HCl solution (chlorine evolution and Mn^{II} formation). Therefore, a chloride ion has to be introduced into the inner coordination sphere of the cobalt in the absence of a permanganate ion—for example, with the preparation of $[\text{Co}(\text{NH}_3)_5\text{Cl}]\text{Cl}_2$ (**compound 4**) [14]—and the outer sphere chloride ions have to be exchanged with permanganate ions, such as occurred with the perrhenate ions in the preparation of **compound 3-Re** [15,16]. A possible reaction route is the reaction of $[\text{Co}(\text{NH}_3)_5\text{Cl}]\text{SO}_4$ [14] with barium permanganate [17–20]; however, this method was not used due to the relatively low solubility of **compound 3-Mn** in water that causes problems in the separation of **compound 3-M** from the insoluble barium sulfate by-product. The reaction of **compound 4** and an excess of NaMnO_4 in a 40% aq. solution, with subsequent cooling to +1 °C resulted in the formation of the **compound 3-Mn** as a reddish-purple precipitate with a 57% yield. Its powder X-ray diffractogram is given in Figure S1. Its solubility in water was 0.0089 M (3.71 g/L) and 0.0225 M (9.39 g/L) at 0 °C and 25 °C, respectively. It is insoluble in aliphatic hydrocarbons and such polar organic solvents like chloroform, dichloromethane, or benzene, but easily soluble in DMF, and decomposes in DMSO.

2.2. Structure of Compound 3-Mn

Dark violet single crystals of **compound 3-Mn** were selected from the precipitate formed during the synthesis. The powder X-ray diffractogram calculated from the SXRD data agreed very well with the experimentally determined powder X-ray diffractogram (Figure S1). Crystallographic data, details of the structure and the refinement results are listed in Table 2, together with the data obtained for the analog perrhenate complex (**compound 3-Re**) [15]. The structural features of **compound 3-Mn** are shown in Figures 1–3. The detailed structural parameters, bond lengths and angles can be found in Tables S1–S3.

Table 2. Crystal data of **compound 3-M**.

Empirical Formula	$[\text{Co}(\text{NH}_3)_5\text{Cl}](\text{MnO}_4)_2$	$[\text{Co}(\text{NH}_3)_5\text{Cl}](\text{ReO}_4)_2 \cdot n\text{H}_2\text{O}$ [15]
Formula Weight	417.4101 g·mol ⁻¹	679.95 g·mol ⁻¹
Crystal System	Orthorhombic	Orthorhombic
Space Group	<i>Cmc</i> 2 ₁	<i>Cmc</i> 2 ₁
Unit cell dimensions, Å	a = 14.2753 (7) b = 14.2816 (6) c = 12.2342 (5);	a = 14.9446 (3) b = 14.6562 (4) c = 12.2434 (4)
Z	8	8
Density (calcd.) (g·cm ⁻³)	2.216	3.368
Temperature (K)	298	293
Volume (Å ³)	2494.24 (19)	2681.68 (13)
R factor (%)	3.67	2.35

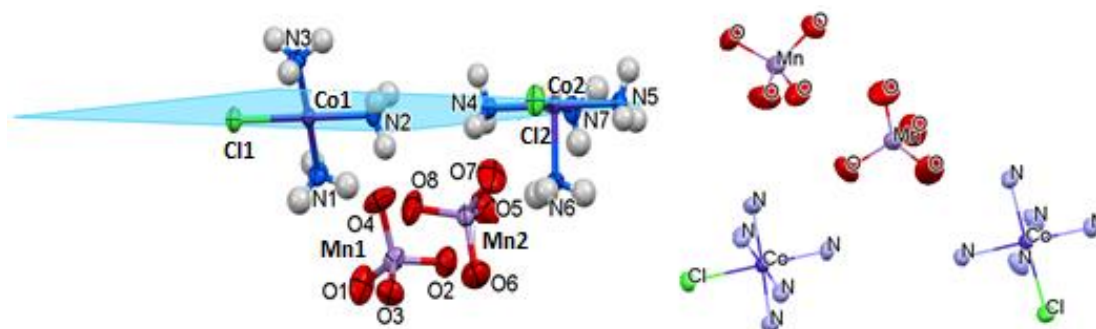


Figure 1. Content of the asymmetric unit of $[\text{Co}(\text{NH}_3)_5\text{Cl}](\text{MnO}_4)_2$ containing two half complex cations and two anions (the light blue plane is a mirror plane cutting the complex cations into two halves; thermal ellipsoids are drawn at a 50% probability level).

Compound 3-M is orthorhombic. Its space group is *Cmc*2₁ (Nr. 36). The coordination around the Co^{3+} cation is octahedral. The asymmetric unit contains two half complex $[\text{Co}(\text{NH}_3)_5\text{Cl}]^{2+}$ cations and two permanganate anions (Figure 1). The central cobalt ions of the complex cations, the coordinated chloride anions, and some of the ammonia ligands sit on a mirror plane and therefore have half-site occupancy, so that the hydrogens of these ammonia molecules are disordered over two mirrored positions. The structural features of **compound 3-Mn** are shown in Figures 1–3.

The axial Co–N bond distance (Co–N1 = 1.955 (6) Å) was shorter in cation A than the equatorial bond distances (1.964(4)–1.965(4) Å), whereas in cation B, the axial Co–N distance (Co–N7 = 1.964 (6) Å) was longer than the equatorial ones (1.950(4)–1.960 (6) Å). The Co–Cl bonds were almost equal (2.258 (2) and 2.255 (2) Å in cation A and B, respectively). The Co–Cl distances in the analogous perrhenate complex (**Compound 3-Re**) were found to be 2.270 (2) and 2.260 (2) Å, whereas the Co–N distances varied between 1.960 (5)–1.972 (6) and 1.948 (7)–1.988 (4) Å, respectively. Layers of the complex cations in the bc plane were embedded within permanganate layers (Figure 2).

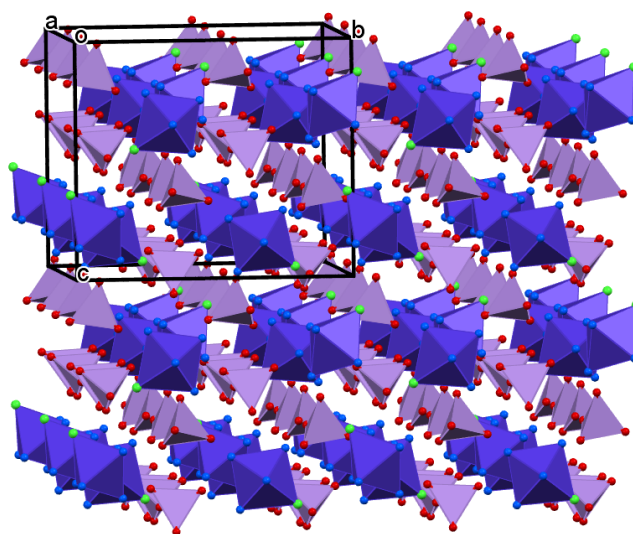


Figure 2. Parallel $[\text{Co}(\text{NH}_3)_5\text{Cl}]^{2+}$ (dark violet octahedra) and MnO_4^- (light violet tetrahedra) layers in the bc plane (view in the direction of the c axis).

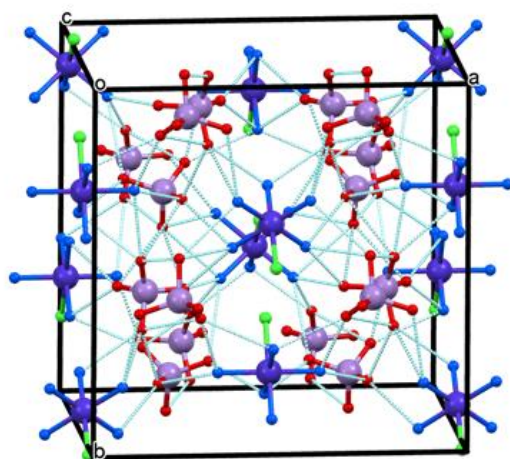


Figure 3. Packing arrangement of $[\text{Co}(\text{NH}_3)_5\text{Cl}](\text{MnO}_4)_2$ and hydrogen bonds in light blue (hanging contacts are omitted for clarity) between the ions.

The $[\text{Co}(\text{NH}_3)_5\text{Cl}]^{2+}$ cation has five hydrogen donor groups and one hydrogen acceptor group. The arrangement of the cations in the crystal lattice is such that all ammonia hydrogens can find at least one acceptor (chloride or permanganate oxygen) (Figure 3, Table S3).

The strengths of $\text{N-H} \dots \text{O}$ and $\text{N-H} \dots \text{Cl}$ hydrogen bonds in **compound 3-Mn** were comparable with the hydrogen bond strengths of the analogous perrhenate complex (**compound 3-Re**) ($\text{N} \dots \text{O}$ distances were between 2.86–3.23 Å and 2.91–3.29 Å, whereas $\text{N} \dots \text{Cl}$ distances were between 2.98–3.60 Å and 3.33–3.53 Å for **compound 3-Mn** and **compound 3-Re**, respectively [15,16]).

2.3. Spectroscopic Properties of Compound 3-Mn

We analyzed the vibrational spectroscopic modes of **compound 3-Mn** by factor group analysis, considering the structure of $[\text{Co}(\text{NH}_3)_5\text{Cl}](\text{MnO}_4)_2$ to be composed of a Co-Cl group, five NH_3 molecules coordinated to Co (four and three crystallographic types at the special and trivial positions C_s and C_1 , respectively), and two types of isolated MnO_4^- anions. The **compound 3-Mn** is orthorhombic ($Cmc2_1$, $Z = 8$), consisting of two types of positions only: general (with trivial symmetry, 1) and special (with symmetry m , yz plane). The unit cell is base-centered. Thus, the primitive cell contains only four motifs, meaning

$Z' = 4$ for the “spectroscopic cell”. This means that there are two quartets of permanganate anions, each at the position of trivial symmetry. The internal of the NH_3 molecules at the special and trivial symmetry positions (C_s and C_1) can be seen in Figure 4. The internal and external vibrations of the permanganate ions and Co-Cl groups (molecular symmetry $C_{\infty v}$), or external vibrations for the NH_3 ligands in **compound 3-Mn**, are presented by Figures S2–S4.

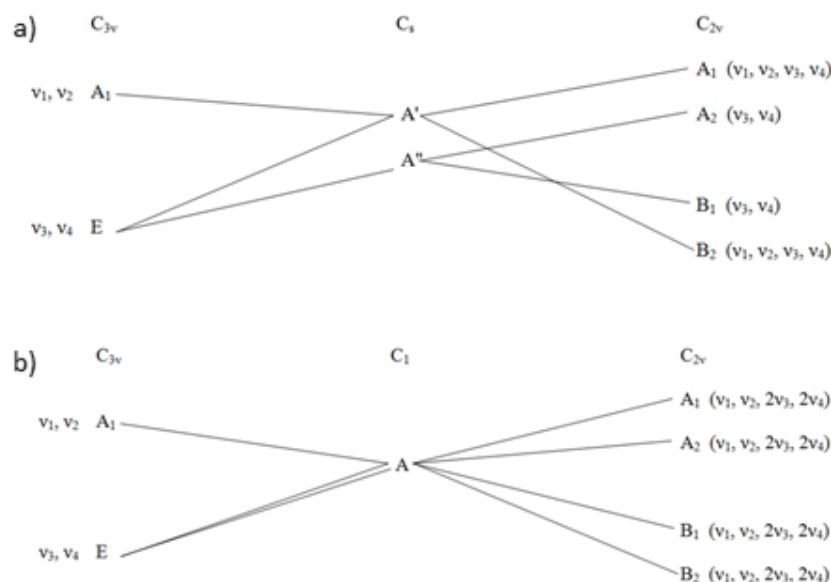


Figure 4. (a) Internal vibrations (four crystallographic types) of NH_3 molecules at special symmetry positions C_s in **compound 3-Mn**; (b) Internal vibrations (three different crystallographic types) of NH_3 molecules at positions of trivial symmetry, C_1 , in **compound 3-Mn**. ν_1 —symmetric stretch.; ν_2 —symmetric bend.; ν_3 —antisymmetric stretch; ν_4 —antisymmetric bend.

2.3.1. Vibrational Modes of the Permanganate Anion

The vibrational modes of the permanganate ion were expected to appear in both the IR and Raman spectra as two series of singlet symmetric (ν_1), triplet antisymmetric (ν_3), doublet symmetric (ν_2) and triplet antisymmetric (ν_4) ones. The IR-forbidden ν_1 and ν_2 under T_d became IR active due to symmetry lowering (C_{2v}) (Figure 5).

The IR, Raman and far-IR spectra of **compound 3-Mn** are given in Figures 4, 5 and S5. The low-temperature Raman spectral range contains the permanganate and $[\text{CoN}_5\text{Cl}]^{2+}$ skeleton vibrations of **compound 3-Mn**, which can be seen in Figure 6. The IR and Raman data assignments can be seen in Tables 3–5.

The low-temperature Raman spectra for **compound 3-Mn** were recorded in the range of $1000\text{--}200\text{ cm}^{-1}$ (Figure 6).

Despite the forbidden nature of $\nu_s(\text{Mn-O})$ and $\delta_s(\text{Mn-O})$ modes in T_d , 2 and 2×2 , weak singlet IR bands, respectively, were expected to appear due to the distortion of the MnO_4^- symmetry (C_{2v}) and the presence of two sets of permanganate ions in the structure; however, the IR spectrum contained one singlet band at 841 cm^{-1} and one at 352 cm^{-1} , assigned as $\nu_s(\text{Mn-O})$ and $\delta_s(\text{MnO})$ modes. The band at 841 cm^{-1} had a shoulder (Figure 5). The $\nu_s(\text{Mn-O})$ mode was expected and found to be an intensive band in the Raman spectrum without splitting at room temperature and as two singlets at 123 K , whereas the $\nu_s(\text{Mn-O})$ appeared as a singlet at room temperature and as a singlet with two shoulders in the low-temperature Raman spectra. The relatively high IR intensity of the $\nu_s(\text{Mn-O})$ band can be attributed to the occurrence of a vibrational mode of the cation core $[\text{Co}(\text{NH}_3)_5\text{Cl}]^{2+}$ located around this wavenumber and coinciding with the $\nu_s(\text{Mn-O})$ band. Abbas [21] and Najar [22] assigned a band around $\sim 844\text{ cm}^{-1}$ to $\nu(\text{Co-Cl})$, whereas Sacconi [23] assigned a band around 849 to $\rho(\text{NH}_3)$ in the IR spectrum of $[\text{Co}(\text{NH}_3)_5\text{Cl}]\text{Cl}_2$ (**compound 4**). Thus,

one of these modes might coincide with the band of $\nu_s(\text{Mn-O})$ and play a role in the appearance of an intensive mixed IR band (a consequence of vibrational resonance). A detailed study of the skeletal vibrational modes [24–26] (see below), including the $\nu(\text{Co-Cl})$ mode, showed that it was located in the far-IR range and not around 844 cm^{-1} . Thus, the coinciding component may only be the $\rho(\text{NH}_3)$ mode. The low-temperature (123 K) Raman spectrum of **compound 3-Mn** showed two bands at 849 and 839 cm^{-1} (Figure 6), with similar intensities. The $\rho(\text{NH}_3)$ mode could not be seen in the Raman spectrum [25] but appeared in the IR spectrum of **compound 4** [21,25]. Thus, the splitting of the singlet Raman band into two components can only be attributed to the appearance of the singlets of two kinds of permanganate ions located in the structure of **compound 3-Mn**. The lack of $\rho(\text{NH}_3)$ band in the Raman spectrum and its role in the increase in the intensity of the mixed $\nu_s(\text{Mn-O}) + \rho(\text{NH}_3)$ IR band were confirmed by the deuteration of **compound 3-Mn** as well. The IR and Raman spectra of the deuterated **compound 3-Mn** (Figures S6–S8) showed that the $\rho(\text{NH}_3)$ component of the mixed IR band was decomposed (the shape of the band at 841 cm^{-1} was changed and a new band appeared at 646 cm^{-1} ($\rho(\text{ND}_3)$)), whereas the $\nu_s(\text{Mn-O})$ band structure in the LT-Raman spectrum was not changed at all by deuteration. The antisymmetric stretching mode ($\nu_{as}(\text{Mn-O})$) was a strong band in the IR and a weak one in the Raman spectra at room temperature (Table 3). The low-temperature Raman study (123 K, Figure 6) showed splitting of the band located around $\sim 900\text{ cm}^{-1}$ into six components, which corresponded to the two sets of triplet $\nu_{as}(\text{Mn-O})(\text{F}_2)$ modes. There were no coinciding cationic modes in this spectral range.

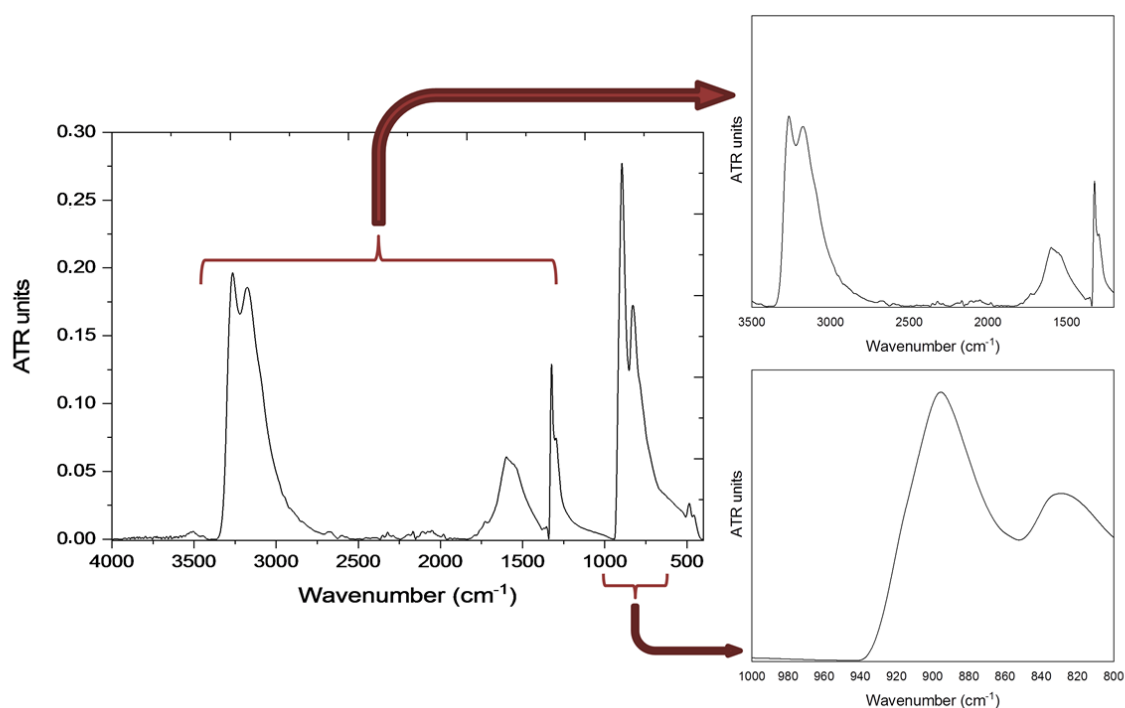


Figure 5. IR spectrum of **compound 3-Mn** in the range of $4000\text{--}400\text{ cm}^{-1}$ at room temperature.

The symmetric deformation mode ($\delta_s(\text{Mn-O})$) was double degenerated, and according to this, $2 \times 2 = 4$ bands were expected both in the far-IR and Raman spectra. The far-IR and the LT-Raman spectra contained one and two bands at 381 and $386/396\text{ cm}^{-1}$, respectively. The intensities of the two bands in the LT-Raman spectrum were almost equal, and the asymmetric shape of the bands showed that these consisted of more than one component. Since $\delta_{s,s}(\text{Mn-O})$ is a double degenerated mode, and there are two sets of permanganate ions in the structure, the two bands probably contain 2 components each. The wide band found at room temperature Raman spectra (Figure 6) split at 123 K. This may be attributed to the appearance of the two sets of permanganate ion modes and due to the splitting of the

E symmetry mode. The antisymmetric $\nu_{as}(\text{Mn-O})$ mode appeared in both the far-IR and the LT-Raman spectra around 349 (sh) and 346 cm^{-1} (Figure 6 and Figure S5), respectively.

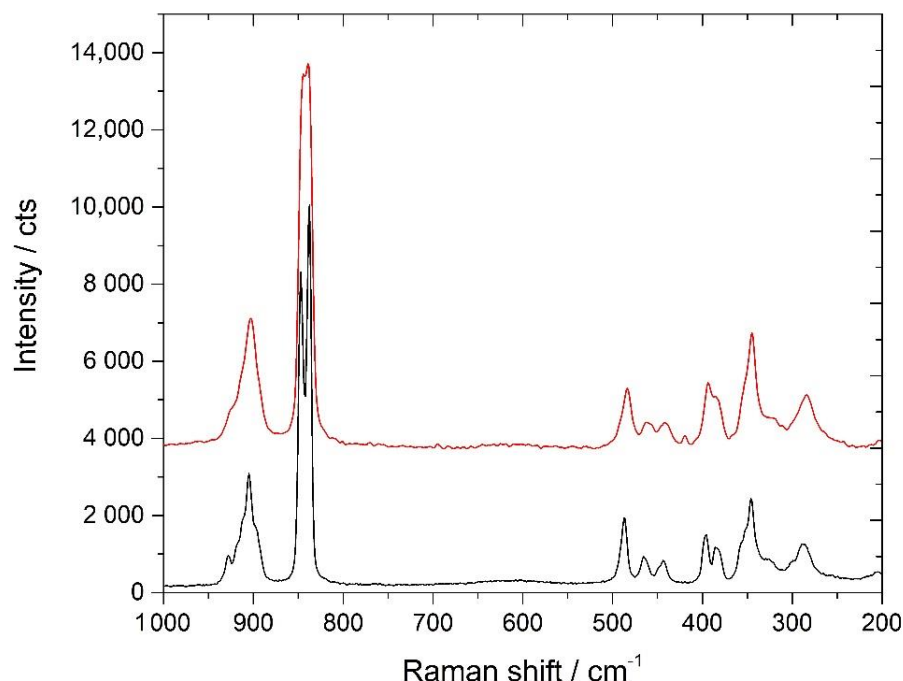


Figure 6. Raman spectra of **compound 3-Mn** at 298 (red) and 123 K (black) in the range of 1000–200 cm^{-1} .

Table 3. Assignments of permanganate ion vibrational modes in the IR and Raman spectra of **compound 3-Mn**.

Band/Assignment	Wavenumber/Raman Shift (cm^{-1})		
	IR	Raman (785 nm)	
		298 K	123 K
ν_1 (MnO), ν_{as} (A) *	829	841	848, 838
ν_3 (MnO), ν_{as} (F_2)	895	903	928, 918sh, 913sh, 905sh, 899sh
ν_4 (MnO), δ_{as} (F_2)	379	389	396, 386, 383
ν_2 (MnO), δ_s (E)	352	346	352sh, 358sh, 346

* Mixed band of ν_1 (Mn-O) and $\rho(\text{NH}_3)$.

2.3.2. Ligand Vibrations

The correlation analysis of the cationic part of **compound 3-Mn** showed seven (4 in C_s and 3 in C_1) and two sets of vibrational modes belonging to ammonia molecules (Figure 4) and Co-Cl groups (Figure S3). The Co-N and Co-Cl modes were evaluated as skeletal modes, and the assignment of the vibrational modes of the ammonia ligands in **compound 3-Mn** and its deuterated form (Figures S6–S8) are given in Table 4.

The differences in the geometrical (axial and equatorial) and the seven crystallographic positions of ammonia molecules resulted in poorly resolved complex band systems for all kinds of N-H modes. The symmetric deformation mode ν_s (N-H) of **compound 3-Mn** showed two main types of ammonia ligated with different strengths to the central Co^{III} -ion. A relative bond strength parameter (ϵ) for the ammonia molecules in ammine complexes was defined by Grinberg [27,28]. The parameter (ϵ) was found to be 0.88 and 0.80 as the two types of coordinated ammonia molecules gave two different δ_s (N-H) bands in the IR spectrum of **compound 3-Mn**. Thus, the bond strength difference between the two main types of coordinated ammonia molecules in **compound 3-Mn** is $\sim 10\%$. This difference may

be attributed to the change in the strength of the Co-N bond (apical or equatorial position); however, the electron density change caused by this difference might be attributed to the difference between the hydrogen bond strength of each ammonia molecule, which can play a crucial role in the value of the Grinberg parameter [2,28].

Table 4. The IR and Raman spectra of the ammonia ligand in $[\text{Co}(\text{NH}_3)_5\text{Cl}](\text{MnO}_4)_2$ (**compound 3-Mn**) and its deuterated form.

Band/Assignment	Wavenumber (cm^{-1})			
	Compound 3-Mn		Deuterated Compound 3-Mn	
	IR, 298 K	Raman (785 nm), 123 K	IR, 298 K	Raman (785 nm), 123 K
$\nu_{\text{as}}(\text{HNH})(\text{DND})$	3293	-	2444	-
$\nu_{\text{s}}(\text{HNH})(\text{DND})$	3270	-	2319	-
$\delta_{\text{as}}(\text{HNH})(\text{DND})$	1607	-	1153	-
$\delta_{\text{s}}(\text{HNH})(\text{DND})$	1324, 1294 (m)	1352, 1311 (vw)	1015	-
$\rho(\text{NH}_3)(\text{ND}_3)$	829 (s)	-	646	-

The positions of N-H stretching and deformation N-H modes in the IR spectrum of **compound 3-Mn** did not give unambiguous information about the presence and strength of hydrogen bonds in the **compound 3-Mn**. The $\rho(\text{NH}_3)$ rocking mode is the most sensitive vibrational mode to detect the presence of hydrogen bonds in ammonia complexes [23], but the $\rho(\text{NH}_3)$ in the IR spectrum of the **compound 3-Mn** was a mixed band with $\nu_{\text{s}}(\text{Mn-O})$. Therefore, we prepared the deuterated **compound 3-Mn** and determined the $\rho(\text{ND}_3)$ band position (646 cm^{-1}). Using the $\rho(\text{NH}_3)/\rho(\text{ND}_3)$ wavenumber ratio found for $[\text{Co}(\text{NH}_3)_5\text{X}]\text{X}_2$ (1.267) compounds [23], we calculated the position of $\rho(\text{NH}_3)$ for **compound 3-Mn** and found it to be 818 cm^{-1} . This showed that the strength of the hydrogen bond in **compound 3-Mn** is weaker than in $[\text{Co}(\text{NH}_3)_5\text{Cl}]\text{Cl}_2$ ($\rho(\text{NH}_3) = 849 \text{ cm}^{-1}$) and is between those found in $[\text{Co}(\text{NH}_3)_5\text{Br}]\text{Br}_2$ ($\rho(\text{NH}_3) = 830 \text{ cm}^{-1}$) and $[\text{Co}(\text{NH}_3)_5\text{I}]\text{I}_2$ ($\rho(\text{NH}_3) = 810 \text{ cm}^{-1}$) [23].

2.3.3. Skeletal Vibrations

The skeletal vibrations were evaluated by the normal coordinate analysis of the $[\text{Co}(\text{NH}_3)_5\text{Cl}]^{2+}$ ion [24–26]. For the skeleton $[\text{Mn}_5\text{X}]^{2+}$, assuming C_{4v} symmetry, 11 normal modes were expected. The A_1 and E species were IR and Raman active, whereas the B_1 and B_2 species were only Raman active. The normal modes and band assignments for **compound 3-M** and its deuterated form are given in Table 5.

Based on the correlation analysis results (Figure S3), two sets of $\nu(\text{Co-Cl})$ modes were expected and found at 278/272sh and 288/285 cm^{-1} in the far-IR (Figure S5) and LT-Raman spectra (Figure 6), respectively. The slight shifts of these bands on deuteration (**compound 3-Mn** and its deuterated form) (average $\nu_{\text{H}}/\nu_{\text{D}} = \sim 1.04$) can be attributed to the coupling of the $\nu(\text{Co-Cl})$ mode with other skeletal vibrational modes. The intensity of some bands was very weak but based on the data of normal coordinate analysis of the $[\text{Co}(\text{NH}_3)_5\text{Cl}]^{2+}$ and $[\text{Co}(\text{ND}_3)_5\text{Cl}]^{2+}$ skeletons, all bands were successfully assigned (Table 5).

2.4. UV-VIS Spectroscopy

The solid-phase UV-VIS spectrum of **compound 3-Mn** was recorded at room temperature, but the spectrum contained strongly overlapping bands both in the UV and visible region (Figure S9). The band at 217 nm may have belonged to both the CT band of the complex cation (electron transfer is from chlorine to the d_{z^2} orbital of cobalt (LMCT)) and the ${}^1\text{A}_1\text{-}{}^1\text{T}_2$ ($t_1\text{-}4t_2$) transition of a permanganate ion as well. The Cl to Co band position for **compound 4** and the ${}^1\text{A}_1\text{-}{}^1\text{T}_2$ ($t_1\text{-}4t_2$) transition for KMnO_4 were found at 227 nm [8,29,30]. A wide band was observed with maximums at 249 and 266, which may have belonged to

the ${}^1A_1-{}^1T_2$ ($3t_2-2e$) and ${}^1T_{2g}-{}^1A_{1g}$ transition of the permanganate ion and the octahedral $[Co(NH_3)_5Cl]^{2+}$ cation [29,30], respectively. The analogous bands were found at 259 and 274 nm for the $KMnO_4$ and **compound 4**, respectively [8,29,30]. Due to the purple color of the complex cation and the permanganate anion in **compound 3-Mn**, the visible region contained a very intensive band system between 500 and 600 nm. The permanganate ${}^1A_1-{}^1T_2$ (t_1-2e) band for the $KMnO_4$ was found between 500 and 562 nm [8], and the doublet of the ${}^1T_{1g}-{}^1A_{1g}$ transition of the $[Co(NH_3)_5Cl]_2SO_4$ was found at 470 and 547 nm [29]. The maximums at 570 (permanganate) and 546 nm (complex cation) for **compound 3-Mn** probably belonged to these transitions. No split of the ${}^1T_{1g}-{}^1A_{1g}$ transition of the complex cation due to the difference between the contribution of the chloride ion ($1Cl + 3NH_3$) and ammonia ($4NH_3$) coordination was observed. The band at 685 nm probably belonged to the ${}^1A_1-{}^1T_1$ (t_1-2e) transition of permanganate ion. This transition was found at 720 nm for the $KMnO_4$ and 710 nm for the $[Agpy_2]MnO_4$ [8].

Table 5. Skeletal vibrational mode assignments in the IR and Raman spectra of **compound 3-Mn** and its deuterated form.

Species	Mode	Assignment	Compound 3-Mn		Deuterated Compound 3-Mn	
			IR (298 K)	Raman (123 K)	IR (298 K)	Raman (123 K)
A ₁ (R IR)	ν_1	ν (Co-Cl)	278, 272sh	288, 285	264	265
	ν_2	ν_s (CoN ₄)	458	465	451	456
	ν_3	ν (Co-N)axial	488	487	483	489
	ν_4	π (Co-N ₄)	199	189sh	185	184
B ₁ (R)	ν_5	ν_{as} (CoN ₄)	-	443	-	448
	ν_6	π (Co-N ₄)	-	193sh	-	193sh
B ₂ (R)	ν_7	δ (NCoN)	-	327	-	327
E (R, IR)	ν_8	ν (Co-N)axial	505, 493 sh	496 sh	483	505
	ν_9	δ (NCoN or CoN ₄ wag)	320	329	344 sh	347
	ν_{10}	δ (NCoCl or CoN ₄ rock)	200	205	199 sh	203
	ν_{11}	δ (NCoN or CoN ₄ in-plane blend)	259sh	265	264	265

2.5. Thermal Decomposition of Compound 3-Mn

The thermal decomposition of [(chlorido)pentaamminecobalt(III)] permanganate (**compound 3-Mn**) was studied in an oxidative and inert atmosphere. There were no significant differences between the decomposition mechanisms in argon and air. The decomposition processes were somewhat more intensive in air than in argon, but the characteristic temperatures were almost the same. Based on the mass losses, powder XRD and the Co:Mn = 1:2 stoichiometry in **compound 3-M**, the final decomposition product above 400 °C was an oxide phase with the overall formula of $CoMn_2O_4$, with an average size of 16.8 nm (identified by powder XRD, and size determined by the Scherrer method (Figure 7)).

The thermal decomposition of **compound 3-Mn** started at 121 °C, onset (Figures S11 and S12). The mass loss in the first decomposition step was ~4.9%, which was somewhat more than the mass percent of one molecule of NH_3 (4.08%).

The IR study supported the notion that the ammonia molecules were bonded with various strengths ($\epsilon = 0.80$ and 0.88 , see above), which predicted a possible stepwise ammonia loss. The TG-MS study, however, unambiguously showed that in the first decomposition step, the leaving product was water ($m/z = 18$, H_2O^+) and not ammonia ($m/z = 17$, NH_3^+) (Figure 8 and Figure S11). The shoulder at around 125 °C on the ion curve $m/z = 17$ corresponded to the HO^+ fragment ion of water. Moreover, the ammonia had a significant $m/z = 16$ peak but the ion intensity curve of $m/z = 16$ did not have any peak or shoulder at around 125 °C. Neither N_2 nor NO_x compounds were formed in this step. **Compound 3-Mn** is anhydrous. Thus, water may only be the reaction product of a solid-phase quasi-intramolecular redox reaction between ammonia as the hydrogen source

and a species containing oxygen. Due to the inert atmosphere, the oxygen source may only be the permanganate ion. Thus, this redox reaction was centered on ammonia ligands and permanganate ions.

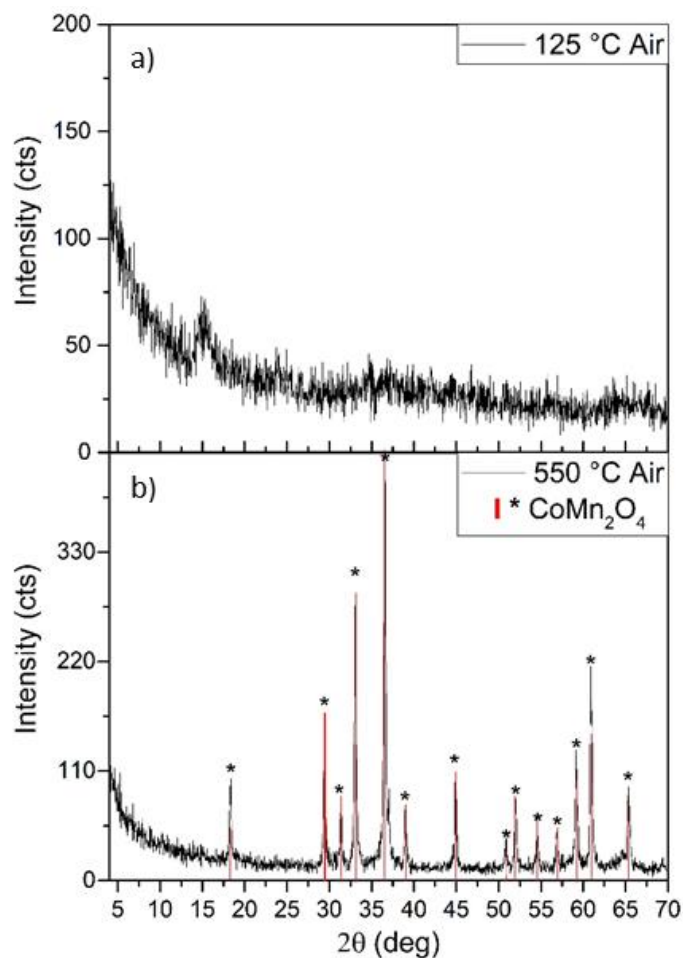


Figure 7. Powder X-ray diffractogram of the decomposition products of **compound 3 Mn** at 125 (a) and 550 °C (b) in 1 h in the air atmosphere.

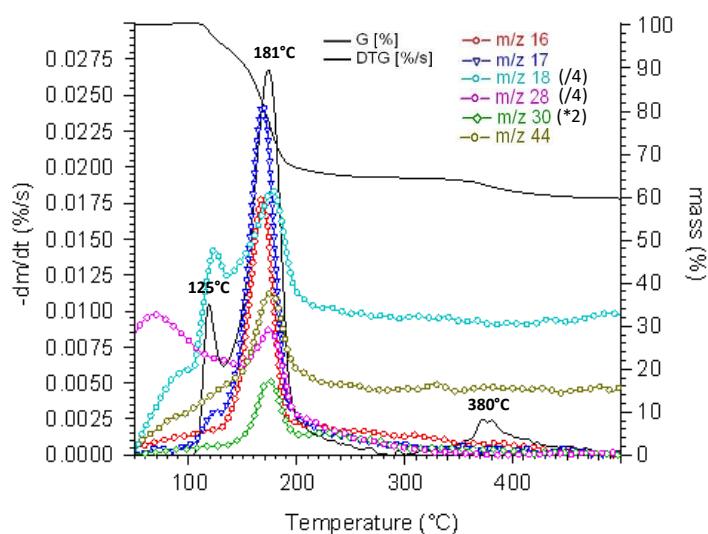


Figure 8. Thermal decomposition curves of **compound 3-Mn** in an argon atmosphere.

The IR spectra of the decomposition product formed from **compound 3-Mn** at 125 °C (Figure 9) showed that the permanganate ion IR bands almost completely disappeared. There were no signs of manganate (VI) or manganate (V) ions [17,19]. Thus, manganese valence in the decomposition product may only be +2, +3, or +4. The release of one water molecule left seven oxygen atoms remaining from the eight oxygen atoms of the two permanganate ions in **compound 3-M**, distributed among the possible redox products. The primary decomposition product was X-ray amorphous, but its IR (Figure 9) and far-IR spectra (Figure S12) showed the presence of an ammonium ion (shoulder at $\sim 1680\text{ cm}^{-1}$ ($\delta_{\text{as}}(\text{N-H})$), $\nu_2 + \nu_4$ combination band at $\sim 2840\text{ cm}^{-1}$) and nitrate ions ($\nu_{\text{as}}(\text{N-O}) \sim 1370\text{ cm}^{-1}$). The N-H bands belonging to $[\text{Co}^{\text{II}}(\text{NH}_3)_4]^{2+}$ ions were expected to appear around the same wavenumbers as the NH_3 bands of **compound 4** [31]. The decomposition intermediate showed the band characteristics for todorokite and related mixed manganese oxide family members as containing $\text{Mn}^{\text{III}}/\text{Mn}^{\text{IV}}$ species [32].

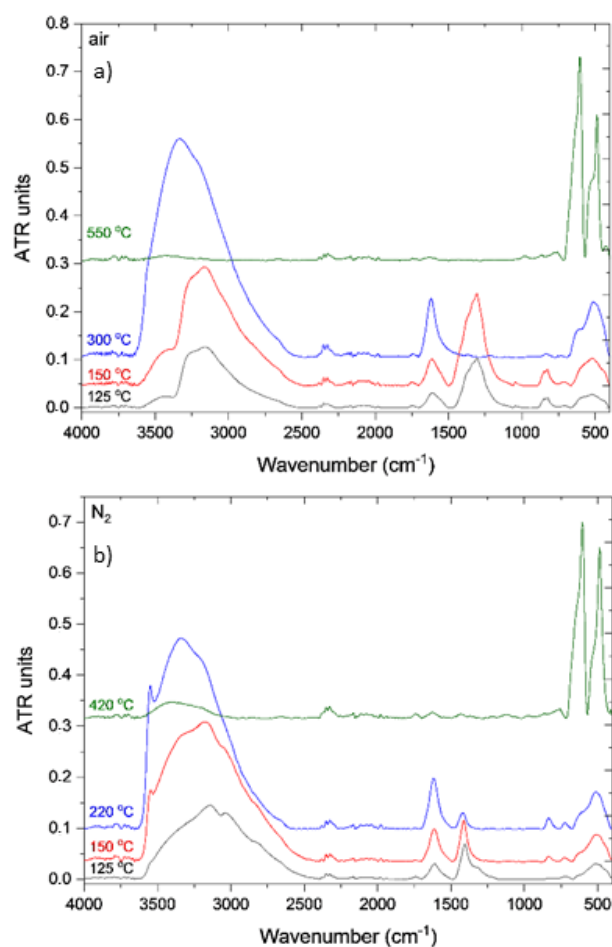


Figure 9. IR spectra of thermal decomposition intermediates of **compound 3-Mn** formed under air (a) and nitrogen (b) atmospheres.

The first thermal decomposition step of the **compound 3-Mn** was also studied in refluxing toluene. The boiling temperature of toluene (110 °C) limits the maximal decomposition reaction temperature by absorbing the evolved reaction heat via the evaporation of toluene, which prevents overheating by the heat of the reaction. The solid phase formed in the thermal decomposition of **compound 3-Mn** under refluxing toluene in 1 h consisted of amorphous phases (Figure 10), which could be crystallized by heating above 400 °C with the formation of CoMn_2O_4 and gaseous (N_2 , H_2O , NH_3 , NH_4Cl) products. The crystallite size of the CoMn_2O_4 depended on the heating time and temperature, similarly to other spinels prepared from ammine complexes of transition metal permanganates [1,3–5].

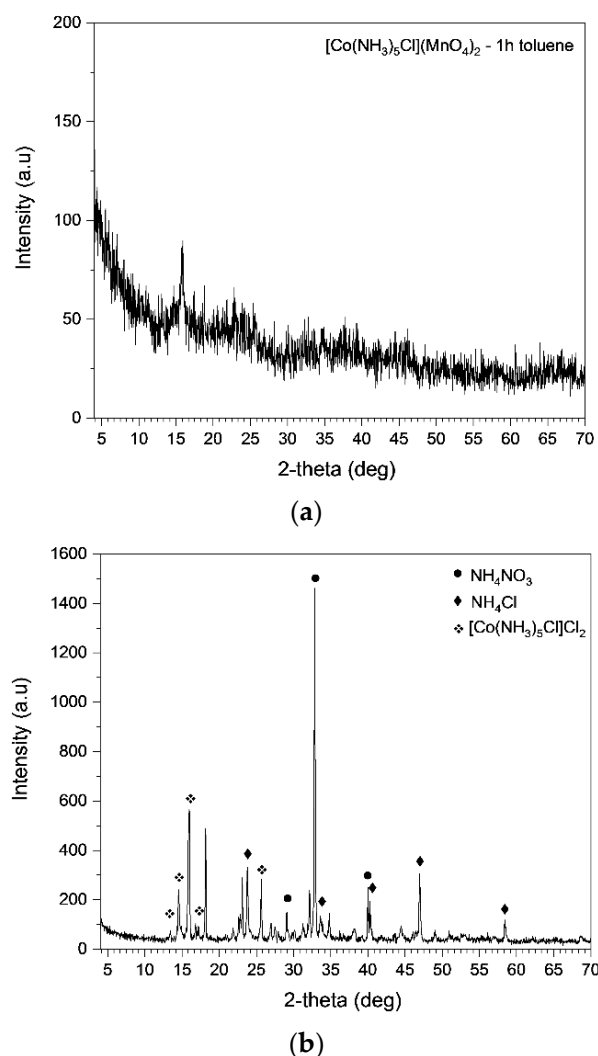


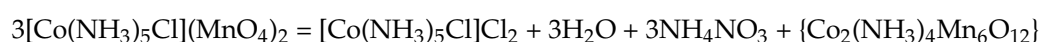
Figure 10. (a) XRD of the decomposition product of **compound 3-Mn** after 1 h reflux in toluene and (b) XRD of the dried aqueous extract of the thermal decomposition product formed under toluene.

Separating the amorphous reaction product into water-soluble and insoluble (oxide) parts and evaporating the aqueous leachate, we assigned the water-soluble components by powder XRD and IR as NH_4NO_3 , $[\text{Co}(\text{NH}_3)_5\text{Cl}]\text{Cl}_2$ (compound 4) and a small amount of NH_4Cl (Figure 10). The NH_4Cl was probably formed as a hydrolysis product of compound 4.

It is well known that ammonium nitrate forms in the solid-phase quasi-intramolecular redox reaction of the ammonia complexes of divalent metal permanganates with the formation of solid Mn (III) type spinel compounds [1–5]:



Neutralizing one charge of the trivalent cobalt in **compound 3-Mn** with a chloride ion results in a formal “divalent complex cation”, and an analog reaction of this “divalent cation” can explain the formation of one mol of water and NH_4NO_3 . The residual solid phase can be characterized with a formal $\{\text{CoClMn}_2\text{O}_4 + 3\text{NH}_3\}$ composition. The material, valence, and charge balances for chlorine, nitrogen, hydrogen, and oxygen, together with the amount of the evolved water, and the lack of ammonia and oxygen evolution, resulted in the following reaction in the first decomposition step:



Since no gaseous ammonia was evolved, the ammonia molecules which were not oxidized to nitrate or protonated to ammonium ions, or were not coordinated in **compound 4**, could be fixed in a coordinated form in the cobalt and manganese-containing residual oxide phase. Depending on the valences of the Co ions ($2 \times \text{III}$, $2 \times \text{II}$ or $\text{II} + \text{III}$), the charge of Co cations can neutralize $\{\text{Mn}_6\text{O}_{12}\}^{n-}$ units with six, four, or five negative charges, thus, according to this, the average valence of manganese was $18/6$ (6Mn^{III}), $20/6$ (4Mn^{III} and 2Mn^{IV}), or $21/6$ (3Mn^{III} and 3Mn^{IV}), respectively. Although there was no sign of ammonia oxidation with Co^{III} in this decomposition step (the lack of N_2 formation confirmed it [33]), the Co^{II} and Mn^{IV} centers in the oxide phase might have been formed due to the valence distribution between the Co^{III} and Mn^{III} . This is a hidden solid-phase quasi-intramolecular redox reaction without mass loss and the formation of other assignable redox products.

The typical coordination number of Co^{III} in its ammonia complexes is 6, and $\text{Co}(\text{II})$ forms stable tetraammine complexes. Thus, the stoichiometry of $\text{Co}:\text{NH}_3$ suggested that one cobalt might be expected to be divalent and complexed with four ammonia molecules. Furthermore, the composition and IR spectrum of the decomposition product (Figures 8 and S11) and the possible charges of the $\{\text{Mn}_6\text{O}_{12}\}^{n-}$ (n may be 4, 5 or 6) unit strongly suggest that $[\text{Co}_2(\text{NH}_3)_4\text{Mn}_6\text{O}_{12}]$ belongs to todorokite or a similar type of manganese oxide family [34]. Todorokite is constructed of triple chains of MnO_6 octahedra forming large tunnels with square cross-sections [34], which can incorporate as large cations as $[\text{Co}(\text{NH}_3)_n]^{2+/3+}$ ($n = 2, 4$ or 6) and free $\text{Co}^{\text{II/III}}$ cations as well.

XPS could not directly determine the $\text{Co}^{\text{II/III}}$ and $\text{Mn}^{\text{II/III}}$ ratio due to the ammonia loss of $[\text{Co}_2(\text{NH}_3)_4\text{Mn}_6\text{O}_{12}]$ in a high vacuum, which led to chemical changes in the studied sample. Therefore, future ^{57}Co Mössbauer studies are planned to investigate the $[\text{Co}_2(\text{NH}_3)_4\text{Mn}_6\text{O}_{12}]$ phase in more detail.

The first thermal decomposition step of **compound 3-Mn** was exothermic in both an oxidative and an inert atmosphere. The reaction heats were found to be 475.85 and 479.95 kJ/mol by DSC (Figure S14a,b) in pure O_2 and N_2 , respectively. Thus, the outer oxygen source did not play any role in the first step of the decomposition process.

In the second decomposition step, the mass loss was $\sim 28.6\%$, and above 300°C , a slight mass loss of 6.5% was observed. The residual mass at 500°C was 57.7% , which was somewhat more than the mass percent of the CoMn_2O_4 spinel (55.77%) (Figure S10).

The TG-MS curves showed simultaneous N_2O and H_2O formation ($m/z = 44$ and 18 , respectively), which is typical in the thermal decomposition of ammonium nitrate:



Based on the $\text{N}_2\text{O}/\text{NO}$ ($m/z = 44$ and 30 , respectively) peak intensity ratios, the formation of NO may be attributed not only to the fragmentation of N_2O [35] but to another NO source as well. The formation of N_2 and ammonia as gaseous products ($m/z = 28$ and $m/z = 17$ or $m/z = 16$, respectively) may be attributed to the decomposition of **compound 4** [33], but the mass loss showed that the $[\text{Co}_2(\text{NH}_3)_4\text{Mn}_6\text{O}_{12}]$ oxide phase also lost ammonia. The intensity ratio of $m/z = 18$ (H_2O^+) and $m/z = 17$ (OH^+ and NH_3^+) in this decomposition step was <1 , which confirmed the ammonia evolution. Therefore, the decomposition product of **compound 4** was NH_3 , NH_4Cl , and N_2 [33]:

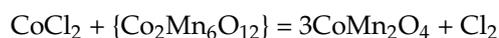


This process was a solid-phase quasi-intramolecular redox reaction centered on Co^{III} and the ammonia ligand. Ammonium chloride (HCl) could not be detected directly due to its fast reaction with the capillary column organic film layer. The reaction heat (Figure S13) was found to be -102.3 and -121.5 kJ/mol in O_2 and N_2 , respectively. This shows that the oxygen gas had an influence on the reaction heat. A similar effect of the outer oxygen was observed in the thermal decomposition of $[\text{Ag}(\text{NH}_3)_2\text{ClO}_4]$ [36]. That was attributed to the forming of NO (its formation was endothermic) in a higher amount than in an inert atmosphere. The second decomposition step of **compound 3-Mn** showed that the

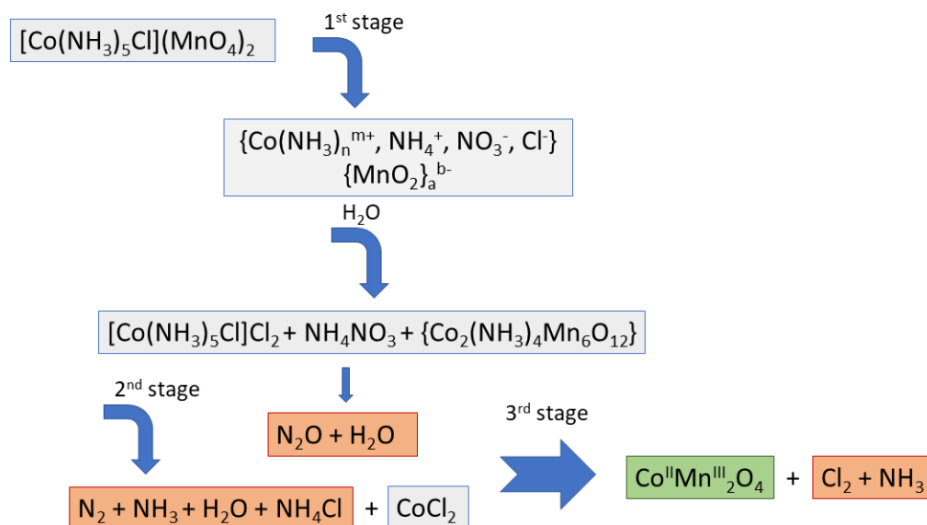
formation of NO ($m/z = 30$), and the presence of Co-Mn oxides can help the oxidation of ammonia with the outer oxygen into NO.

In the second decomposition step of **compound 3-Mn** (~180 °C), the previously formed NH_4NO_3 , $[\text{Co}(\text{NH}_3)_5\text{Cl}]\text{Cl}_2$ and $\{\text{Co}_2(\text{NH}_3)_4\text{Mn}_6\text{O}_{12}\}$ phases decomposed in simultaneous processes. The thermal decomposition temperature of $[\text{Co}(\text{NH}_3)_5\text{Cl}]\text{Cl}_2$ (**compound 4**) with N_2 and NH_3 formation (175 °C) [34] agreed well with the peak temperature of the second decomposition step (181 °C). The decomposition reaction of **compound 4** may initiate the decomposition of both ammonium nitrate (catalyzed by the oxide phases present [37–39]) and $\{\text{Co}_2(\text{NH}_3)_4\text{Mn}_6\text{O}_{12}\}$ simultaneously.

The third decomposition step around 340 °C was the reaction of the cobalt(II) chloride and $[\text{Co}_2(\text{NH}_3)_4\text{Mn}_6\text{O}_{12}]$ intermediates with the formation of cobalt manganese oxide (CoMn_2O_4), which contained formally one Co^{II} and two Mn^{III} ions. Two manganese (IV) ions or two cobalt (III) ions can oxidize two chloride ions into chlorine according to the reaction:



The mass loss of the third decomposition step was slightly higher than the mass losses calculated for $1/3 \text{Cl}_2$ due to the release of the residual ammonia. Still, the overall mass loss agreed well with the CoMn_2O_4 formation. Some amount of chlorine ($m/z = 35 \text{Cl}^+$) was also detected, in the argon without NO_2 formation whereas in the air it was together with NO_2 formation (Figure S11). The decomposition process is summarized in Scheme 1. As Scheme 1 shows, the only solid final decomposition product was CoMn_2O_4 . Thus, the temperature-controlled decomposition of **compound 3-Mn** is an easy way to prepare nanosized cobalt manganite with $\text{Co}:\text{Mn} = 1:2$ stoichiometry.



Scheme 1. Thermal decomposition of **compound 3-Mn**. Grey: solid intermediates; brown: gaseous decomposition products; green: solid decomposition product.

The stoichiometry of the third decomposition step requested the presence of two Mn^{IV} or two Co^{III} ions (or one Mn^{III} and one Co^{III}), which could oxidize two chloride ions into chlorine. Consequently, $4 \text{Mn}^{\text{III}} + 2 \text{Mn}^{\text{IV}} + 2 \text{Co}^{\text{II}}$, $5 \text{Mn}^{\text{III}} + \text{Mn}^{\text{IV}} + \text{Co}^{\text{III}} + \text{Co}^{\text{II}}$, or $6 \text{Mn}^{\text{III}} + 2 \text{Co}^{\text{III}}$ ions (the oxidizing constituents are italicized) may have neutralized the negative charges of the framework oxygens in the $[\text{Co}_2(\text{NH}_3)_4\text{Mn}_6\text{O}_{12}]$. Thus, the $\{\text{Co}_2(\text{NH}_3)_4\text{Mn}_6\text{O}_{12}\}$ intermediate phase consisted of todorokite-like $\{\text{Mn}_4^{\text{III}}\text{Mn}_2^{\text{IV}}\text{O}_{12}\}_n^{4n-}$, $\{\text{Mn}_5^{\text{III}}\text{Mn}^{\text{IV}}\text{O}_{12}\}_n^{5n-}$ or $\{\text{Mn}_6^{\text{III}}\text{O}_{12}\}_n^{6n-}$ frameworks, which embedded $2 \times n$ (Co^{II} and/or Co^{III}) cations in their tunnels, respectively. Ammonia ligands ($4 \times n$) were coordinated to cobalt ions. The two cobalt ions may have been intercalated in the tunnels as one $\text{Co}^{\text{II,III}} + \text{one } \text{Co}^{\text{II,III}}(\text{NH}_3)_4^{2+}$ ion, or two $[\text{Co}^{\text{II,III}}(\text{NH}_3)_2]^{2/3+}$ ions. Co^{III} typically forms hexacoordinated, whereas Co^{II} forms tetraordinated ammonia complexes, thus, the most

probable formula contained a tetraamminecobalt (II) cation or ammonia-bridged Co (III) structural units, but the structure of this decomposition intermediate requires further detailed investigation.

The last decomposition reaction was influenced by oxygen, which means that oxygen defects ($\text{CoMn}_2\text{O}_{4+\delta}$) can be expected if the decomposition is completed in the presence of oxygen. Since the oxygen defects may play a role in the desired catalytic activity of Co-Mn oxides, the CoMn_2O_4 samples prepared in both an inert atmosphere and air were tested as photocatalysts in the UV degradation of Congo red.

2.6. Surface Characterization of the Thermal Decomposition Products of Compound 3-Mn and Their Photocatalytic Activity in Congo Red Degradation

Twice were the three decomposition intermediates and the two final decomposition products prepared by isothermal heating of **compound 3-Mn** at 125, 150, 220 and 420 °C under N_2 , and at 125, 150, 300 and 550 °C in air. The morphology of the end product (spinel-like) obtained at 420 °C (N_2) and at 550 °C (air) was similar and can be seen in Figure 11.

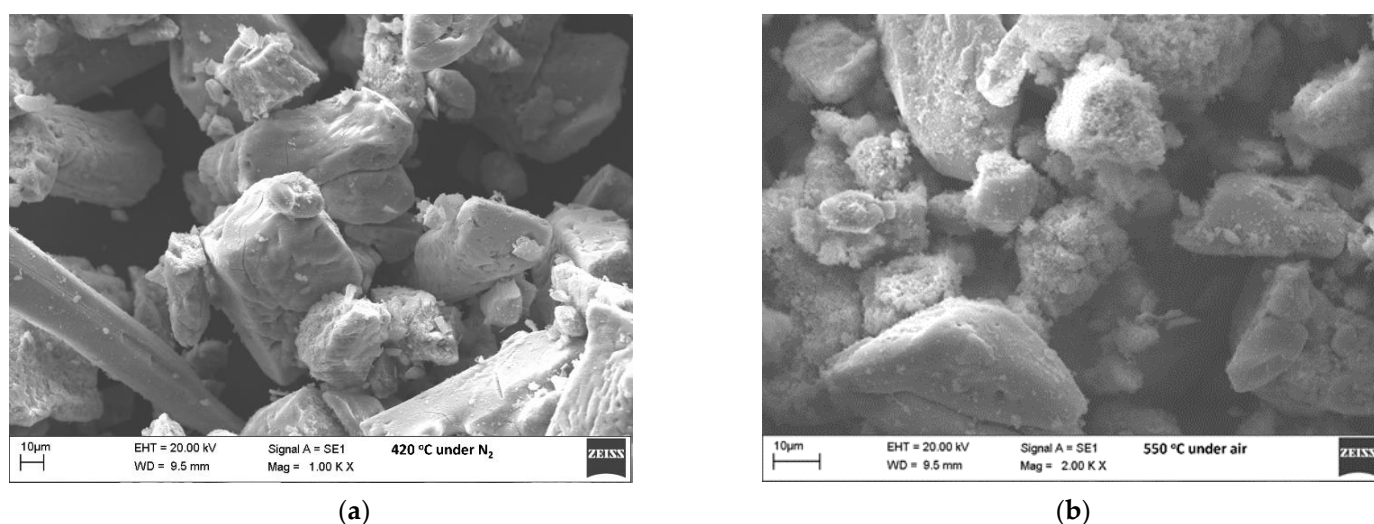


Figure 11. SEM images of the decomposition products formed at 420 °C under nitrogen (a) and at 550 °C under air (b).

The specific surface area of each intermediate and the final product was measured (Table 6).

Table 6. The specific surface area of intermediates formed at different temperatures under air and N_2 .

T °C (N_2)	125	150	220	420
SSA ($\text{m}^2 \cdot \text{g}^{-1}$)	130	118	176	32
T °C (air)	125	150	300	500
SSA ($\text{m}^2 \cdot \text{g}^{-1}$)	22	23	194	23

SSA: specific surface area.

The specific surface area of the decomposition intermediates formed under N_2 changed irregularly, and the lowest surface area ($\sim 32 \text{ m}^2 \cdot \text{g}^{-1}$) was found after crystallization and the sintering of the amorphous primary reaction products at 420 °C. Under an oxidizing atmosphere, there was an expansion in the bulk phase up to 300 °C, and then, the surface area decreased again due to crystallization and sintering at 550 °C ($23 \text{ m}^2 \cdot \text{g}^{-1}$).

The first intermediate was obtained at 125 °C under both atmospheres and the end products were produced at 420 °C under nitrogen and at 550 °C in air. We checked

their potential as a photocatalyst in the degradation of organic dyes. Our findings are summarized in Figure 12 and the apparent decomposition rate for each intermediate can be seen in Table 7.

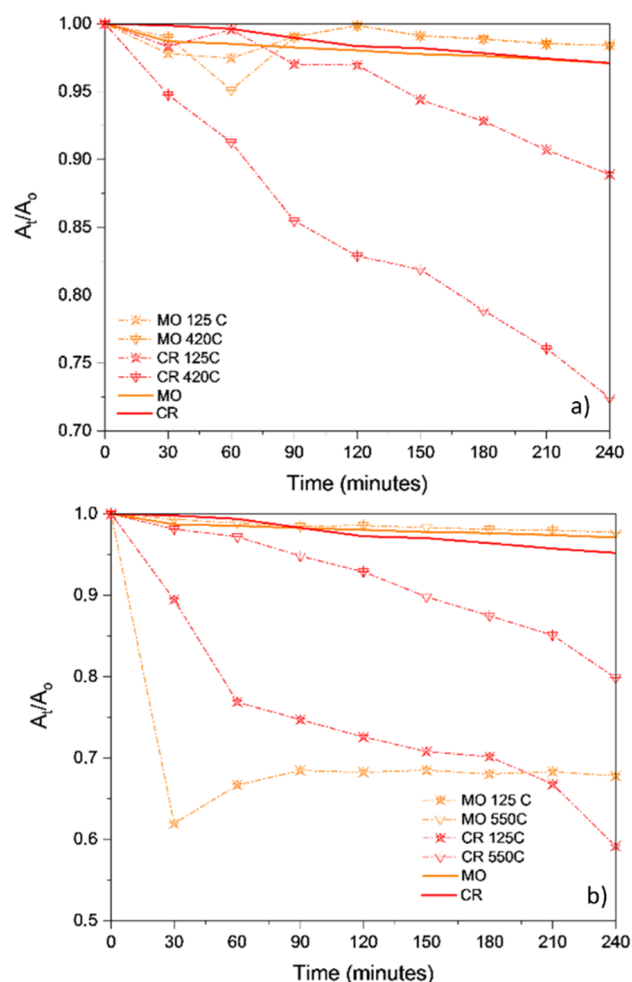


Figure 12. Photocatalysis of decomposition intermediates formed at various temperatures under nitrogen (a) and air (b) during the decomposition of Congo red.

Table 7. Photocatalytic parameters in the decomposition of methyl orange and Congo red with intermediates forming in different conditions.

Substrate	pH	$K_{app}/10^{-4} \cdot \text{min}^{-1}$	R^2
Congo Red, $2 \cdot 10^{-5}$ M, without catalyst	5.7	1.0	0.99
Congo red, $2 \cdot 10^{-5}$ M, with compound 3-Mn at 125 °C in N_2	5.7	5.0	0.93
Congo red, $2 \cdot 10^{-5}$ M, with compound 3-Mn at 125 °C in air	5.7	18.0	0.89
Congo red, $2 \cdot 10^{-5}$ M, with compound 3-Mn at 420 °C in N_2	5.7	13.0	0.98
Congo red, $2 \cdot 10^{-5}$ M, with compound 3-Mn at 550 °C in air	5.7	9.0	0.96

The photocatalyst candidates formed under an inert atmosphere and air during the thermal decomposition of compound 3-Mn showed activity in accelerating the decomposition rate of Congo red. The decomposition of methyl orange in our experiments did not reach any significant level. The end product (CoMn_2O_4) forming under N_2 had higher photoactivity (13 times faster degradation rate compared to the uncatalyzed process) in Congo red degradation by UV light than the intermediate $[\text{Co}_2(\text{NH}_3)_4\text{Mn}_6\text{Mn}_2\text{O}_{12}]$. The intermediate that formed in air at 125 °C accelerated the photodegradation of Congo red

18 times, whereas the final decomposition product (550 °C–air) resulted in only a 9-fold acceleration.

The differences in the chemical character and photocatalytic activity of samples prepared in an aerial and inert atmosphere can be attributed to the differences between the distribution and chemical environment of the low valence (Co^{II} , Mn^{II}) and oxidized (Co^{III} , $\text{Mn}^{\text{III,IV}}$) centers in the studied materials.

3. Materials and Methods

Chemical-grade basic cobalt carbonate, sodium permanganate (40% aq. soln.), ammonia and hydrochloric acid and chemicals containing the isotope (D_2O , DCl in D_2O , ND_4Cl , and ND_3 in D_2O solution) were supplied by Deuton-X Ltd., Érd, Hungary.

Synthesis of compound 4 [14]

Basic cobalt carbonate—20 g of $\text{CoCO}_3 \cdot n\text{Co}(\text{OH})_2 \cdot \text{H}_2\text{O}$ —was dissolved in a 1:1 HCl solution. Then the solution was filtered and chilled. A solution of 250 mL of cc. ammonia and 50 g of $(\text{NH}_4)_2\text{CO}_3$ in 250 mL of distilled water was added. Then, the mixture was oxidized for three hours in a stream of air. Then, 150 g of NH_4Cl was added to the previous solution and the mixture was evaporated until a syrup consistency was obtained. To drive off the CO_2 , a dilute (10%) HCl solution was added. Then, to ensure the basicity of the reaction mixture, 10 mL of cc. ammonia was also added. The mixture was heated until all the solutions became clear, then 300 mL of cc. HCl was added, and the mixture was heated for 1 h. At the end of the process, the crude $[\text{Co}(\text{NH}_3)_5\text{Cl}]\text{Cl}_2$ was precipitated by cooling. The precipitate was filtered off, washed with 1:1 HCl until it was free of NH_4Cl , and then with alcohol until it was free of acid. To purify the crude salt, we dissolved 10 g of powdered crude $[\text{Co}(\text{NH}_3)_5\text{Cl}]\text{Cl}_2$ in 75 mL of distilled water and 50 mL of aqueous NH_3 (10%) in an Erlenmeyer flask covered with a watch glass under heating and stirring. Then, the deep-red solution was filtered and acidified with oxalic acid to be weakly acidic, and some additional $(\text{NH}_4)_2\text{C}_2\text{O}_4$ was added to complete the precipitation. The slurry was allowed to stand and the precipitated, $[\text{Co}(\text{NH}_3)_5(\text{H}_2\text{O})]_2(\text{C}_2\text{O}_4)_3 \cdot 4\text{H}_2\text{O}$ was filtered off and washed with cold water and dried at room temperature. To obtain the pure **compound 4**, 20 g of $[\text{Co}(\text{NH}_3)_5(\text{H}_2\text{O})]_2(\text{C}_2\text{O}_4)_3 \cdot 4\text{H}_2\text{O}$ was dissolved in 150 mL of diluted (2%) aq. ammonia solution in an ice bath, and the insoluble luteo oxalate, $[\text{Co}(\text{NH}_3)_6]_2(\text{C}_2\text{O}_4)_3 \cdot 4\text{H}_2\text{O}$, was filtered off. The filtrate was precipitated in an ice bath with the addition of a 10% aq. HCl solution. The [chloridopentaamminecobalt(III)] chloride (**compound 4**) was filtered off, washed successively with alcohol, absolute alcohol and ether, and dried in air.

Synthesis of compound $[\text{Co}(\text{NH}_3)_5\text{Cl}](\text{MnO}_4)_2$ (**compound 3-Mn**)

To prepare **compound 3-Mn**, we dissolved 1.0 g of $[\text{Co}(\text{NH}_3)_5\text{Cl}]\text{Cl}_2$ in 150 mL of distilled water and 5 mL of a NaMnO_4 solution was added. Then the mixture was heated to 60 °C and stirred for 15 min. Finally, the mixture was cooled to 1 °C. The precipitate that formed was filtered off and dried at room temperature in a desiccator containing CaO . The yield was 57%.

Synthesis of deuterated compounds 4 and 3-Mn

The deuterated **compound 4** could be prepared in three ways: (1) using anhydrous CoCl_2 , ND_4Cl , and ND_3 , and D_2O according to the method described in [24]; (2) via deuteration of $[\text{Co}(\text{NH}_3)_5\text{Cl}]\text{Cl}_2$ dissolved in D_2O and DCl and evaporated to dryness at room temperature in the presence of freshly prepared CaO ; and (3) dissolving **compound 4** in D_2O and freeze-drying the solution to obtain $[\text{Co}(\text{ND}_3)_5(\text{D}_2\text{O})]\text{Cl}_3$, which was converted into deuterated **compound 4** by heating in a high vacuum at 80 °C, according to Sacconi's method [23]. All three ways gave the deuterated **compound 4**, but the deuteration of **compound 4** with D_2O required a large amount of D_2O because of the low solubility of **compound 4** in H_2O (D_2O) (5.2 g/L at 25 °C [40]). The deuteration process was repeated 4 times, then the $[\text{Co}(\text{ND}_3)_5\text{Cl}]\text{Cl}_2$ was dissolved in a minimum quantity of D_2O and reacted with 2 equiv. of KMnO_4 dissolved in D_2O at 60 °C. Then the mixture was cooled, and the deuterated **compound 3-Mn** was isolated as described for the **non-deuterated 3-Mn**.

Elemental Analysis

The cobalt and manganese content of the sample was determined by atomic emission spectroscopy with a Spectro Genesis ICP-OES (SPECTRO Analytical Instruments GmbH, Kleve, Germany) spectrometer. A multielement standard solution (Merck Chemicals GmbH, Darmstadt, Germany) was used for calibration.

The ammonia content of the starting compound and the ammonia/ammonium-ion content of the decomposition intermediates were determined by gravimetry as $(\text{NH}_4)_2\text{PtCl}_6$ (ammonia was liberated by an alkaline treatment and boiling). Due to the redox by-reactions that appeared on heating of the **compound 3-M** which produced NO_x gases, the absorption of the evolved ammonia in mineral acid solutions and titrating back the excess acid could not be used due to HNO_2 and HNO_3 formation.

The evolved ammonia/oxidized ammonia ratio was measured by the isotherm heating of the starting complex at a given temperature with the absorption of ammonia in the H_2PtCl_6 solution. The NO_x and N_2 gases did not give a precipitate with H_2PtCl_6 , whereas the ammonia formed insoluble orange-colored $(\text{NH}_4)_2\text{PtCl}_6$.

Vibrational Spectroscopy

The far-IR and FT-IR spectra of the crystalline **compound 3-Mn** and its deuterated form were recorded in ATR (attenuated total reflection) mode on a BioRad-Digilab FTS-30-FIR and a Bruker Alpha IR spectrometer for the 400–40 and 4000–400 cm^{-1} range, respectively. Raman measurement (298 and 123 K) of **compound 3-Mn** and its deuterated form were performed on a Horiba Jobin-Yvon LabRAM microspectrometer with an external 785 nm diode laser source (~80 mW) coupled to an Olympus BX-40 optical microscope. In the low-temperature measurements, a Linkam THMS600 temperature-controlled microscope stage was used. The laser beam was focused on an objective of 20 \times . In order to avoid the thermal degradation of **compound 3-Mn**, we used a D0.6 (123 K) and a D2 (298 K) intensity filter to decrease the laser power to 25% and 1%, respectively. The confocal hole of 1000 μm and monochromators with 950 groove mm^{-1} grating were used for light dispersion. The spectral range of 2000–100 cm^{-1} was selected with a resolution of 4 cm^{-1} . The exposure times were 60 s to produce intensive peaks.

The UV-VIS DRS (UV-VIS diffuse reflectance spectrum) of **compound 3-Mn** was measured at room temperature with a Jasco V-670 UV-VIS spectrophotometer equipped with a NV-470 integrating sphere (BaSO_4 standard as reference).

Scanning Electron Microscopy

A JEOL JSM-5500LV scanning electron microscope was used in the experiments. The specimens were fixed on sample holders (Cu/Zn alloy with a carbon tape) and sputtered with a conductive layer (Au/Pd) for imaging.

Powder X-ray diffractometry

A Philips PW-1050 Bragg-Brentano para-focusing goniometer was used, equipped with a Cu cathode operated at 40 kV and 35 mA with a secondary beam graphite monochromator and a proportional counter. Scans were recorded in step mode. The diffraction patterns were evaluated with a full profile fitting technique.

Single-crystal X-ray diffraction

A dark violet needle of $[\text{Co}(\text{NH}_3)_5\text{Cl}](\text{MnO}_4)_2$ (**compound 3-Mn**) was mounted on a loop. Single crystal X-ray diffraction measurements were carried out on an Agilent Supernova diffractometer equipped with a dual-sealed X-ray tube source, a kappa goniometer and a position-sensitive detector at room temperature. An Mo source was used in a hemisphere of the reciprocal space up to the resolution of 0.65 Å. Data was collected with the CrysAlis1 software. The structure was solved and refined with the SHELX software package2 from Olex23. The atomic positions were determined by direct methods, while hydrogen atomic positions were calculated from assumed geometries. Hydrogen atoms were included in the structure factor calculations, but they were not refined. The isotropic displacement parameters of the hydrogen atoms were approximated from the $U(\text{eq})$ value of the atom they were bonded to.

Thermal studies

Thermal data were collected with a modified TGS-2 thermobalance (Perkin Elmer, USA) coupled to a HiQuad quadrupole mass spectrometer (Pfeiffer Vacuum, Germany). Approximately 1 mg samples were measured in a platinum sample pan. Decomposition was followed from ambient temperature to 500 °C at a 20 °C min⁻¹ heating rate in argon or air as the carrier gas (flow rate = 140 cm³ min⁻¹). Selected significant ions between $m/z = 2-88$ were monitored in the selected ion monitoring (SIM) mode.

The other set of thermal data were collected with a TA Instruments SDT Q600 thermal analyzer coupled to a Hiden Analytical HPR20/QIC mass spectrometer. Decomposition was followed from room temperature to 500 °C at a heating rate of 5 °C min⁻¹ in argon as the carrier gas (flow rate = 50 cm³ min⁻¹) and at a heating rate of 2 °C min⁻¹ in air as the carrier gas (flow rate = 50 cm³ min⁻¹). The sample holder and the reference were the same alumina crucible. A sample mass of ~1 mg was mixed with Al₂O₃ to avoid an explosive decomposition of the sample. Selected ions between $m/z = 1-83$ were monitored in multiple ion detection modes (MIDs).

The non-isothermal DSC curves between -130 and 300 °C were recorded with a Perkin Elmer DSC 7 apparatus. The sample masses were between 3 and 5 mg and the samples were tested at a heating rate of 5 °C/min under a continuous nitrogen flow (20 cm³ min⁻¹) in an unsealed aluminum pan.

4. Conclusions

1. An unknown cobalt(III) complex with chlorido and ammonia ligands, [Co(NH₃)₅Cl](MnO₄)₂ (**compound 3-Mn**), was synthesized. This complex is a precursor to nano-sized Co-manganite with Co:Mn = 1:2 stoichiometry and an average size of 16.8 nm.
2. The vibrational modes in **compound 3-Mn** were studied in detail and the overlapping bands were assigned via deuteration and low-temperature Raman measurements.
3. The structure of **compound 3-Mn** was revealed with single-crystal X-ray diffraction and the 3D-hydrogen bonds were evaluated.
4. The hydrogen bonds between the N-H hydrogen atoms and the Mn-O oxygen atoms acted as redox centers to initiate a solid-phase quasi-intramolecular redox reaction even at 120 °C involving the Co^{III} centers and permanganate ion as the oxidants and ammonia as a reductant. An amorphous precursor of [Co(NH₃)₅Cl]Cl₂, NH₄NO₃, and a todorokite-like compound contains {Mn₄^{III}Mn^{IV}O₁₂}_n⁴ⁿ⁻, {Mn₅^{III}Mn^{IV}O₁₂}_n⁵ⁿ⁻ or {Mn₆^{III}O₁₂}_n⁶ⁿ⁻ frameworks with 2 × n (Co^{II} and/or Co^{III}) cations, and 4 × n ammonia ligand in their tunnels.
5. The decomposition intermediates formed at ~120 °C and decomposed on heating via a series of redox reactions with the formation of such redox products as Co^{II}Mn^{III}₂O₄ spinel, N₂, N₂O and Cl₂.
- 6) The only solid was the nanosized (16.8 nm) CoMn₂O₄, with a Co:Mn = 1:2 stoichiometry.
6. The thermal decomposition reaction of **compound 3-Mn** consisted of a series of solid-phase quasi-intramolecular redox reactions consisting of various redox pairs such as permanganate ions and ammonia ligands, Co(III) and Mn(III), Co(III) and ammonia, or nitrate and ammonium ions.
7. The prepared CoMn₂O₄ spinel had photocatalytic activity in Congo red degradation with UV light. The activity of CoMn₂O₄ depended on its synthesis conditions such as temperature or atmosphere. Congo red degradation was 9 and 13 times faster in the presence of CoMn₂O₄ prepared at 520 °C (in air) or 450 °C (under N₂), respectively.

Supplementary Materials: The following supporting information can be downloaded at: <https://www.mdpi.com/article/10.3390/inorganics10020018/s1>, Figure S1: Comparison of experimental powder X-ray diffractogram and a calculated one (from data of single crystal measurement) of the **compound 3-Mn**; Figure S2: Correlation analysis for the internal and external vibrations of permanganate ion in **compound 3-Mn**; Figure S3: Correlation analysis for the internal and external vibrations of Co-Cl groups (molecular symmetry C_{∞v}) in **compound 3-Mn**; Figure S4: Correlation analysis for the external vibrations of ammonia ligands in **compound 3-Mn**; Figure S5: Far-IR spectrum of

compound 3-Mn in the range of 400–100 cm^{-1} at room temperature; Figure S6: Far-IR spectrum of the deuterated **compound 3-Mn** in the range of 400–100 cm^{-1} at room temperature; Figure S7: IR spectrum of the deuterated **compound 3-Mn** in the range of 4000–400 cm^{-1} at room temperature; Figure S8: Raman spectra of the deuterated **compound 3-Mn** in the range of 1100–100 cm^{-1} at 123 and 298 K; Figure S9: UV-VIS spectrum of **compound 3-Mn**; Figure S10: TG-DTG-DTA curves of **compound 3-Mn** in argon (a) and air (b) atmosphere; Figure S11: Selected TG-MS curves of **compound 3-Mn** in air (a) ($m/z = 35, \text{Cl}^+; m/z = 30 (\text{NO}^+); m/z = 46, \text{NO}_2^+; m/z = 18, \text{H}_2\text{O}^+; m/z = 17 \text{OH}^+, \text{NH}_3^+$) and argon (b) atmosphere ($m/z = 35, \text{Cl}^+; m/z = 30 (\text{NO}^+); m/z = 18, \text{H}_2\text{O}^+; m/z = 17 \text{OH}^+, \text{NH}_3^+$); Figure S12: Far-IR spectra of the thermal decomposition intermediates formed from **compound 3-Mn** in air (a) and inert (b) atmosphere; Figure S13: DSC analysis of **compound 3-Mn** in pure oxygen (a) and nitrogen (b); Table S1: Crystal data and structure refinement of **compound 3-M**; Table S2: Bond lengths (\AA) and angles ($^\circ$) in **compound 3-Mn**; Table S3: Analysis of potential hydrogen bonds and schemes with $d(\text{D} \dots \text{A}) < R(\text{D}) + R(\text{A}) + 0.50$, $d(\text{H} \dots \text{A}) < R(\text{H}) + R(\text{A}) - 0.12 \text{ \AA}$, $\text{D-H} \dots \text{A} > 100.0 \text{ Deg}$ in the crystal of $[\text{Co}(\text{NH}_3)_5\text{Cl}](\text{MnO}_4)_2$ (distances are given in \AA).

Author Contributions: Conceptualization, F.P.F. and L.K.; methodology, F.P.F., K.A.B. and L.K.; software, F.P.F.; formal analysis, V.M.P.; investigation, F.P.F., É.K., Z.C., L.B., B.B.H., K.A.B. and A.F.; resources, I.M.S. and K.A.B.; data curation, V.M.P. and L.K.; writing—original draft preparation, F.P.F. and L.K.; writing—review and editing, F.P.F., K.A.B., V.M.P. and L.K.; visualization, L.B. and F.P.F.; supervision, L.K.; project administration, I.M.S.; funding acquisition, K.A.B., I.M.S. and L.K. All authors have read and agreed to the published version of the manuscript.

Funding: The research was supported by the European Union and the State of Hungary, co-financed by the European Regional Development Fund (VEKOP-2.3.2-16-2017-00013) (LK) and the ÚNKP-21-3 New National Excellence Program of the Ministry for Innovation and Technology from the source of the National Research, Development and Innovation Fund (KAB).

Institutional Review Board Statement: Not applicable.

Informed Consent Statement: Not applicable.

Conflicts of Interest: The authors declare no conflict of interest.

References

1. Solt, H.E.; Németh, P.; Mohai, M.; Sajó, I.E.; Klébert, S.; Franguelli, F.P.; Fogaca, L.A.; Pawar, R.P.; Kótai, L. Temperature-Limited Synthesis of Copper Manganites along the Borderline of the Amorphous/Crystalline State and Their Catalytic Activity in CO Oxidation. *ACS Omega* **2021**, *6*, 1523–1533. [[CrossRef](#)] [[PubMed](#)]
2. Fogaca, L.A.; Kovács, É.; Németh, G.; Kamarás, K.; Berés, K.A.; Németh, P.; Petruševski, V.; Bereczki, L.; Holló, B.B.; Sajó, I.E.; et al. Solid-Phase Quasi-Intramolecular Redox Reaction of $[\text{Ag}(\text{NH}_3)_2]\text{MnO}_4$: An Easy Way to Prepare Pure AgMnO_2 . *Inorg. Chem.* **2021**, *60*, 3749–3760. [[CrossRef](#)] [[PubMed](#)]
3. Kótai, L.; Baneerji, K.K.; Sajó, I.; Kristof, J.; Sreedhar, B.; Holly, S.; Keresztury, G.; Rockenbauer, A. An unprecedented-type intramolecular redox reaction of solid tetraamminecopper(2+) bis(permanganate)- $[\text{Cu}(\text{NH}_3)_4](\text{MnO}_4)_2$ —A low-temperature synthesis of copper dimanganese tetraoxide-type (CuMn_2O_4) nanocrystalline catalyst precursors. *Helv. Chim. Acta* **2002**, *85*, 2316–2327. [[CrossRef](#)]
4. Sajó, I.E.; Kótai, L.; Keresztury, G.; Gács, I.; Pokol, G.; Kristóf, J.; Soptrayanov, B.; Petruševski, V.; Timpu, D.; Sharma, P.K. Studies on the Chemistry of Tetraamminezinc(II) Dipermanganate ($[\text{Zn}(\text{NH}_3)_4](\text{MnO}_4)_2$): Low-Temperature Synthesis of the Manganese Zinc Oxide (ZnMn_2O_4) Catalyst Precursor. *Helv. Chim. Acta* **2008**, *91*, 1646–1658. [[CrossRef](#)]
5. Kótai, L.; Sajó, I.E.; Jakab, E.; Keresztury, G.; Németh, C.; Gács, I.; Menyhárd, A.; Kristóf, J.; Hajba, L.; Petruševski, V.; et al. Studies on the chemistry of $[\text{Cd}(\text{NH}_3)_4](\text{MnO}_4)_2$. A low-temperature synthesis route of the $\text{CdMn}_2\text{O}_{4+x}$ type NO_x and CH_3SH sensor. *Z. Anorg. All. Chem* **2012**, *638*, 177–186. [[CrossRef](#)]
6. Mansouri, M.; Atashi, H.; Tabrizi, F.F.; Mirzaei, A.A.; Mansouri, G. Kinetics studies of nano-structured cobalt-manganese oxide catalysts in Fischer-Tropsch synthesis. *J. Ind. Eng. Chem.* **2013**, *19*, 1177–1183. [[CrossRef](#)]
7. Franguelli, F.P.; Berés, K.A.; Kótai, L. Pyridinesilver Tetraoxometallate Complexes: Overview of the Synthesis, Structure, and Properties of Pyridine Complexed AgXO_4 ($\text{X} = \text{Cl}, \text{Mn}, \text{Re}$) Compounds. *Inorganics* **2021**, *9*, 79. [[CrossRef](#)]
8. Kovács, G.B.; May, N.V.; Bombicz, P.A.; Klébert, S.; Németh, P.; Menyhárd, A.; Novodárszki, G.; Petruševski, V.; Franguelli, F.P.; Magyari, J.; et al. An unknown component of a selective and mild oxidant: Structure and oxidative ability of a double salt-type complex having $\kappa^1\text{O}$ -coordinated permanganate anions and three- and four-fold coordinated silver cations. *RSC Adv.* **2019**, *9*, 28387–28398. [[CrossRef](#)]
9. Mansouri, G.; Mansouri, M. Synthesis and characterization of Co-Mn nanocatalyst prepared by thermal decomposition for Fischer-Tropsch reaction. *Iran. J. Chem. Eng.* **2018**, *37*, 1–9.

10. Alvisi, G.U. Ricerche sui Perclorati. Perclorati di Luteocobaltiammine ed osservazioni sui metalloammoni. *Gazz. Chim. Ital.* **1901**, *31*, 289–301.
11. Klobb, T. Contribution à l'étude des sels lutéocobaltiques. *Bull. Soc. Chim. Paris* **1901**, *25*, 1022–1031.
12. Krestov, G.A.; Yatsimirsikii, K.B. Thermodynamical characteristics of (chloro)(pentaamine)cobalt type complex compounds. *Zh. Neorg. Khim.* **1961**, *6*, 2294–2303.
13. Linhard, M.; Weigel, M. Über Komplexverbindungen XXII. Lichtabsorption von Halogeno-pentammin-Co(III)-komplexen im Rot und nahen U.R. *Z. Phys. Chem.* **1957**, *11*, 308–317. [[CrossRef](#)]
14. Jorgensen, S.M. Beiträge zur Chemie der Kobaltammoniakverbindungen; I. Ueber die Chloropurpurekobaltsalze. *J. für Prakt. Chemie.* **1878**, *18*, 209–247. [[CrossRef](#)]
15. Baidina, I.A.; Filatov, E.Y.; Makotchenko, E.V.; Smolentsev, A.I. Synthesis and structure investigation of Co(III) complex salts with the perhenate ion. *J. Struct. Chem.* **2012**, *53*, 112–118. [[CrossRef](#)]
16. Shubin, Y.; Filatov, E.; Baidina, I.; Yusenko, K.; Zadesenetz, A.; Korenev, S.V. Synthesis of $[M(NH_3)_5Cl](ReO_4)_2$ ($M = Cr, Co, Ru, Rh, Ir$) and investigation of thermolysis products. Crystal structure of $[Rh(NH_3)_5Cl](ReO_4)_2$. *J. Struct. Chem.* **2006**, *47*, 1103–1110. [[CrossRef](#)]
17. Kótai, L.; Gács, L.; Sajó, I.E.; Sharma, P.K.; Banerji, K.K. Beliefs and facts in permanganate chemistry—and overview on the synthesis and the reactivity of simple and complex permanganates. *Trends. Inorg. Chem.* **2011**, *11*, 25–104. [[CrossRef](#)]
18. Kótai, L.; Sajó, I.E.; Gács, L.; Pradeep, K.S.; Banerji, K.K. Convenient routes for the preparation of barium permanganate and other permanganate salts. *Z. Anorg. All. Chem.* **2007**, *633*, 1257–1260. [[CrossRef](#)]
19. Kótai, L.; Keszler, A.; Pató, J.; Holly, S.; Banerji, K.K. The reaction of barium manganate with acids and their precursors. *Ind. J. Chem. A.* **1998**, *38A*, 966–968.
20. Kótai, L.; Banerji, K.K. An improved method for the preparation of high-purity permanganate salts. *Synth. React. Inorg. Met. Org. Chem.* **2001**, *31*, 491–495. [[CrossRef](#)]
21. Abbas, N.K.; Habeeb, M.A.; Algidsawi, A.J.K. Preparation of chloropentaamminecobalt (III) chloride and study of its influence on the structural and some optical properties of polyvinyl acetate. *Int. J. Polym. Sci.* **2015**, 926789.
22. Najar, M.H.; Majid, K. Synthesis, characterization, electrical and thermal properties of nanocomposite of polythiophene with nanophotoadduct: A potent composite for electronic use. *J. Mater. Sci. Mater. Electron.* **2013**, *24*, 4332–4339. [[CrossRef](#)]
23. Sacconi, B.L.; Sabatini, A.; Cans, P. Infrared Spectra from of Some Metal-Ammine Complexes. *Inorg. Chem.* **1964**, *3*, 1772–1774. [[CrossRef](#)]
24. Fleming, G.D.; Tellez, C. Estudo espectroscópico vibracional dos complexos $[Co(NH_3)_5X]X_2$ ($X = Cl, Br$) com substituição isotópica H/D. (I): Análise de baixa energia. *Semin. Cienc. Biol. Saúde* **1982**, *12*, 263–267.
25. Loehr, T.M.; Zinich, J.; Long, T.V. The laser-Raman spectra of hexaamminecobalt(III), chloropentaamminecobalt(III), and trans-dichlorotetraamminecobalt(III). *Chem. Phys. Lett.* **1970**, *7*, 183–186. [[CrossRef](#)]
26. Chen, Y.; Christensen, D.H.; Sorensen, G.O.; Nielsen, O.F.; Pedersen, E.B. The skeletal vibrational spectra and metal-ligand force constants of cobalt(III) ammine complexes. *J. Mol. Struct.* **1993**, *299*, 61–72. [[CrossRef](#)]
27. Grinberg, A.A.; Varshavskii, Y.S. The frequency of coordinated ammonia deformation mode and its relationship with the chemical properties of transition metal ammonia complexes. *Primen. Molekul. Spekt. Khim.* **1966**, 104–107.
28. Bereczki, L.; Fogaca, L.A.; Durvanger, Z.; Harmat, V.; Kamarás, K.; Németh, G.; Holló, B.B.; Petruševski, V.; Bódis, E.; Farkas, A.; et al. Dynamic disorder in the high-temperature polymorph of bis[iamminesilver(I)] sulfate—reasons and consequences of simultaneous ammonia release from two different polymorphs. *J. Coord. Chem.* **2021**, *74*, 2144–2162. [[CrossRef](#)]
29. Mitsutsuka, Y.; Kondo, I.; Nakahara, M. Splitting parameters in Ligand field absorption bands of cobalt(III) ammine complexes with chloro or aqua ligands. *Bull. Chem. Soc. Japan* **1986**, *59*, 2767–2771. [[CrossRef](#)]
30. Yamatera, H. Charge-transfer spectra in metal complexes, especially in halogenopentamminecobalt(III) ions. *J. Inorg. Nucl. Chem.* **1960**, *15*, 50–62. [[CrossRef](#)]
31. Muller, A.; Christophliemk, P.; Tossidiss, I. Struktur thermisches Verhalten und eigenschaften von tetramminokobalt(II)-perhenat $[Co(NH_3)_4](ReO_4)_2$; elektronen-und schwingungsspektre. *J. Mol. Struct.* **1973**, *15*, 289–299. [[CrossRef](#)]
32. Potter, R.M.; Rossman, G.R. The tetravalent manganese oxides: Identification, hydration and structural relationships by infrared spectroscopy. *Am. Mineral.* **1979**, *64*, 1199–1218.
33. Wendland, W.W.; Smith, J.P. The thermal decomposition of metal complexes—VII a thermomagnetic study of the Co(III)~Co(II) reduction in cobalt(III) ammine complexes. *J. Inorg. Nucl. Chem.* **1963**, *25*, 1267–1272. [[CrossRef](#)]
34. Turner, S.; Buseck, P.R. Todorokites: A new family of naturally occurring manganese oxides. *Science* **1981**, *212*, 1024–1027. [[CrossRef](#)] [[PubMed](#)]
35. Kocsis, T.; Magyar, J.; Sajó, I.E.; Pasinszki, T.; Homonnay, Z.; Szilágyi, I.M.; Farkas, A.; May, Z.; Effenberger, H.; Szakall, S.; et al. Evidence of quasi-intramolecular redox reactions during thermal decomposition of ammonium hydroxodisulfiteferriate(III), $(NH_4)_2[Fe(OH)(SO_3)_2]H_2O$. *J. Therm. Anal. Calorim.* **2018**, *132*, 493–502. [[CrossRef](#)]
36. Fogaça, L.A.; Bereczki, L.; Petruševski, V.M.; Barta-Holló, B.; Franguelli, F.P.; Mohai, M.; Béres, K.A.; Sajó, I.E.; Szilágyi, I.M.; Kótai, L. A quasi-intramolecular solid-phase redox reaction of ammonia ligands and perchlorate anion in diamminesilver(I) perchlorate. *Inorganics* **2021**, *9*, 38. [[CrossRef](#)]
37. Han, Z.; Sachdeva, S.; Papadaki, M.I.; Mannan, M.S. Ammonium nitrate thermal decomposition with additives. *J. Loss Prev. Process Ind.* **2015**, *35*, 307–315. [[CrossRef](#)]

38. Chaturvedi, S.; Dave, P.N. Review on thermal decomposition of ammonium nitrate. *J. Energetic Mater.* **2013**, *31*, 1–26. [[CrossRef](#)]
39. Muniz, F.T.L.; Miranda, M.A.R.; Dos Santos, C.M.; Sasaki, H.M. The Scherrer equation and the dynamical theory of X-ray diffraction. *Acta Crystallogr. Sect. A Found. Advances.* **2016**, *72*, 385–390. [[CrossRef](#)]
40. Brønsted, J.N.; Delbanco, A.; Volqvartz, K. Über die Bedeutung des Lösungsmittels für die Löslichkeit von Salzen und die Aktivitätskoeffizienten der Ionen. *Z. Für Phys. Chemie.* **1932**, *162*, 128–146. [[CrossRef](#)]